Process Safety and Environmental Protection 187 (2024) 240–248

Contents lists available at ScienceDirect

Process Safety and Environmental Protection

journal homepage: www.journals.elsevier.com/process-safety-and-environmental-protection

Experimental investigation on the behavior of thermal super insulation materials for cryogenic storage tanks in fire incidents

Robert Eberwein [a,*,1], Aliasghar Hajhariri [a], Davide Camplese [b,2], Giordano Emrys Scarponi [b,3], Valerio Cozzani [b,4], Frank Otremba [a,5]

[a] Bundesanstalt für Materialforschung und -prüfung, Unter den Eichen 87, Berlin 12205, Germany
[b] LISES – Laboratory of Industrial Safety and Environmental Sustainability, DICAM – Department of Civil, Chemical, Environmental and Materials Engineering, University of Bologna, Via U. Terracini 28, Bologna 40131, Italy

ARTICLE INFO

Keywords:
Liquefied hydrogen
Liquefied natural gas
Cryogenic storage tank
Fire
Thermal insulation
Multi-Layer Insulation
Perlite
Rock wool
Microspheres

ABSTRACT

The number of vehicles using or transporting cryogenic fuels such as Liquefied Hydrogen (LH2) or Liquefied Natural Gas (LNG) increases fast in the land transportation sector. Does this also entail new risks? The storage of cryogenic fuels requires tanks with Thermal Super Insulations (TSI) to keep the fluid cold and limit the formation of boil-off gas. TSI has proven itself in some applications since the middle of the 20th century, but in the land transport sector they are still quite new, where accidents involving fires, collisions, and their combination are to be expected. This work focuses on investigating the behavior of different types of TSI while exposed to a heat source representing a fire. To this aim, a High-Temperature Thermal Vacuum Chamber (HTTVC) was applied, which allows the thermal loading of a thermal insulation material in a vacuum and measuring the heat flow transported through the TSI in parallel. In this study, the results of 6 samples are presented regarding 3 types of MLI, rock wool, perlites, and microspheres. The thermal exposure caused different effects on the samples. In practice, this can be connected to the rapid release of flammable gases as well as to a Boiling Liquid Expanding Vapour Explosion (BLEVE). These results are relevant for reducing the risks to people and infrastructures in the progressive establishment of tanks for cryogenic fluids in our industry and society. The data presented in the study can be used to improve the design of tanks and TSIs, the assessment of accident scenarios, and the development of measures for first responders.

1. Introduction

The importance of tanks for storing cryogenic fluids is increasing in the energy industry because of the implementation of more environmentally friendly energy sources (IEA, 2022). Key representatives for the application of cryogenic tanks are natural gas in the form of Liquefied Natural Gas (LNG) and hydrogen, e. g. in the form of Liquefied Hydrogen (LH2), for which significantly higher transport capacities can be achieved with the same transport volume using cryogenic storage than with storage based solely on overpressure (Adler and Martins, 2023).

All fluids transported under cryogenic conditions must be kept at very low temperatures for a prolonged time. Hence heat flows into the fluid must be minimized. Thermal Super Insulations (TSI) based on e. g. Multilayer Insulations (MLI), perlites, microspheres, and vacuum are utilized for this purpose and have already proven themselves suitable in some applications (Peschka, 1992; Lisowski and Lisowski, 2018). However, each sector, such as land transport, has its challenges. In this context, car accidents with collisions, fires, and their combination are typical scenarios for which there is insufficient knowledge today about the course and consequences of real scenarios with tanks for cryogenic fluids. Reasons for this are the still short period of use in the land transport, the still low transport volumes, as well as the still few

* Corresponding author.
E-mail address: Robert.eberwein@bam.de (R. Eberwein).
[1] 0000–0003-3134–7456
[2] 0009–0005-4957–2039
[3] 0000–0002-5187–597X
[4] 0000–0003-4680–535X
[5] 0000–0002-1352–0406

https://doi.org/10.1016/j.psep.2024.04.131
Received 11 January 2024; Received in revised form 20 March 2024; Accepted 28 April 2024
Available online 30 April 2024

Nomenclature

A	Surface area
N	Total number of layers of an MLI
$\dot{Q}$, $\dot{Q}_1$, $\dot{Q}_2$, $\dot{Q}_f$	Heat flow
T, T_1, T_2, T_{fi}, T_{fo}	Temperature
c_f	Specific heat capacity
$\dot{m}_f$	Mass flow
n	Index of a layer in an MLI
ε, ε_1, $\varepsilon_2, \varepsilon_{eff}, \varepsilon_{n1}$, ε_{n2}	Emissivity
σ	Stefan-Boltzmann constant

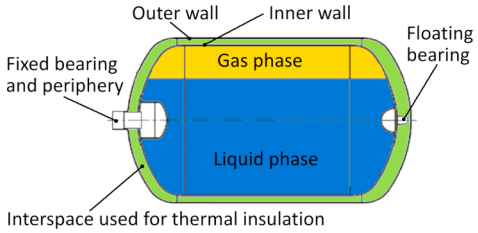

Fig. 1. Scheme of a double-walled tank, typically used for the storage of cryogenic fluids in land transport.

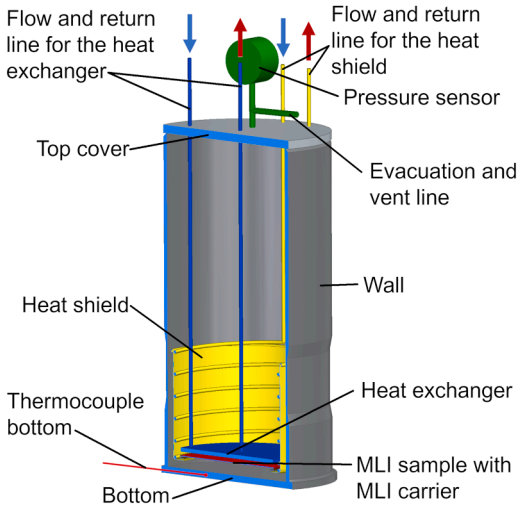

Fig. 2. HTTVC in a sectional view.

documented incidents, and their still low number of losses (Planas, 2004; Planas, 2015; Vollmacher, 2018, Konersmann et al., 2014). However, as the number of transports increases, so does the absolute number of incidents and the risk for higher losses.

The reduction of risks is based on the continuous improvement of codes and standards for design, operation, and handling procedures for first responders, and requires knowledge about the process of the incident (Bradley et al., 2021; Pehr, 1996a; Scarponi et al., 2017; Tugnoli et al., 2012), and wide knowledge about the individual properties of the fluid, as the para-ortho transformation of hydrogen, that can affect an incident (Salzano et al., 2020).

From the research point of view, several papers deal with the effects of vacuum loss in the insulation of tanks for the storage of liquid helium (LHe) (Lehmann and Zahn, 1978; Cavallari et al., 1989; Wiseman et al., 1994) and Liquid Hydrogen (LH2) (Xu et al., 2023). During the development of vehicles fueled with LH2 in the passenger car segment, BMW carried out crash tests, vacuum fracture tests, and fire tests (Pehr, 1996b; Bartlok, 2006), of which only a few details have been published. Further research was done in the LNG Safety Program from the Dutch National LNG Platform, in which, among emergency response, the effects of fires on a vacuum/perlites and a rock wool insulated tank designed for LNG was researched (Kamperveen et al., 2016). Similarly, three tanks for LH2 were tested in the SH2IFT Project (van Wingerden, 2022): two tanks equipped with vacuum/perlites TSI and one equipped with a vacuum/MLI TSI. Based on some of these experiments empirical and numerical studies were published, addressing the time to failure estimation (Ustolin et al., 2021), the behavior of the cryogenic fluid inside the tank as a consequence of fire (Iannaccone et al., 2021), an explosion (Ustolin et al., 2022a,b) and its consequence (Ustolin et al., 2023), the consequences of releases of cryogenic fluids in the environment (Eberwein, 2021; Horvat, 2018; Jäkel, 2018; Luan et al., 2023). Furthermore, some studies are dealing with the behavior of insulation material under heat exposure. Here, Camplese et al. (2023) investigated the effect of heat on parts of MLI under atmospheric conditions, and Eberwein et al. (2023) presented a methodology for the thermal exposure of TSI samples at industrial conditions, which was based on a hydrocarbon fire, and applied to polyester-based MLI.

Table 1
Names and details of the tests.

Name	Description
MLI type 1	10 layers of polyester foil, 12 μm thick, double-sided aluminized with 400 Å, perforated with an open area of 0.075%, interleaved with 9 layers of polyester-fleece material. Overall nominal area-specific weight of 0.308 kg/m^2.
MLI type 2	10 layers of pure aluminium foil, 9 μm thick, interleaved with 9 layers of glass-fleece material. Overall nominal area-specific weight of 0.526 kg/m^2.
MLI type 3	10 layers of pure aluminium foil, 9 μm thick, interleaved with 9 layers of glass-paper material. Overall nominal area-specific weight of 0.390 kg/m^2.
Rock wool	120 mm overall thickness. Overall nominal area-specific weight of 12.1 kg/m^2.
Perlite	120 mm overall thickness. Overall nominal area-specific weight of 14.4 kg/m^2.
Microspheres	120 mm overall thickness of microscopic hollow spheres from borosilicate glass, with particle diameters between 44 μm and 200 μm. Overall nominal area-specific weight of 15 kg/m^2.
Pretest	No filling material in the HTTVC. For more details see Eberwein et al. (2023).

The focus of this study is to compare the behavior of different types of TSI under industrial conditions as a result of their exposure to a heat source reproducing a fire. This can lead to an increase of the heat flow into a tank by several orders of magnitude, permanent damage of the TSI, and a release of flammable gas, as well as a Boiling Liquid Expanding Vapour Explosion (BLEVE). For this purpose, a High-Temperature Thermal Vacuum Chamber (HTTVC) was used as presented in detail in Eberwein et al. (2023), that enables thermal loading of TSI under vacuum conditions and simultaneous measurement of heat flow through the TSI itself. Within the study, different TSIs are tested: three types of MLI, perlites, rockwool, and microspheres.

The results are relevant for the evaluation of accident scenarios involving full-scale cryogenic tanks for LH2 or LNG for instance, and can thus contribute to the improvement of TSI, the development of safer tank designs, as well as the development and definition of emergency measures for the protection of persons and infrastructures.

2. Tank design and heat flux

Land transport comes typically with limited volumetric space and the aim to maximize the payload. The double-walled tank design is particularly suitable to meet these requirements (Peschka, 1992; Mital et al., 2006), which is schematically presented in Fig. 1.

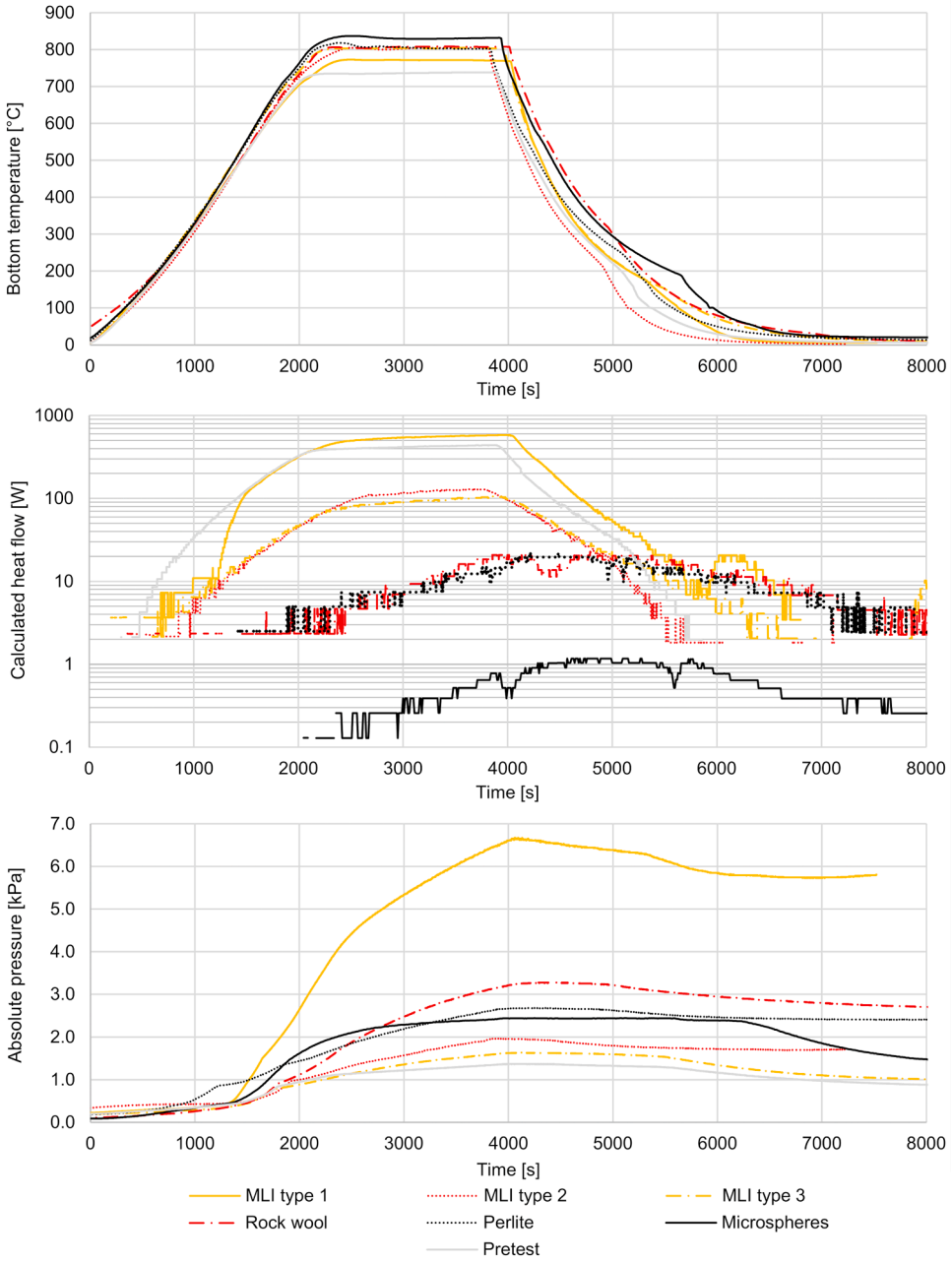

Fig. 3. Bottom temperature, calculated heat flow between bottom and heat exchanger, and measured absolute pressure within the HTTVC, over time.

This design is based on an outer tank in which an inner tank is held by a floating and a fixed bearing. The inner tank contains the cryogenic fluid. The fixed bearing serves as the tank periphery through which the cryogenic fluid is loaded and unloaded. The outer and inner wall form the double wall, whose interspace is used to host the TSI. The filling material for the interspace of the double wall can be of different nature: foam, bulk-fill, and layered, which is often supplemented by vacuum. The combination of a fill material with a vacuum reduces heat flows from the environment into the stored cryogenic fluid by convection, conduction, and radiation. Bulk materials, such as rock wool, perlite, or microspheres are typically applied in large-scale and stationary applications. In small-scale applications, e.g. laboratory or mobile applications, layered systems with vacuum such as multilayer insulations (MLI) have shown better performances in terms of space, thermal insulation, and mass (Lisowski and Lisowski, 2018; Peschka, 1992; Mital et al., 2006). Therefore, the importance of MLI-based TSI for tanks in the land transport sector is high.

Radiation represents the most important heat transfer mechanism in a TSI based on a vacuum and a fill material. Radiation represents a heat flux $\dot{Q}$ emitted by a surface to the surrounding space considering the emissivity ε, area A, and Temperature T in K of the surface and the Stefan-Boltzmann constant with 5.67…x10^{-8} W/(m^{2}K^4) which can be estimated by Eq. (1).

$$\dot{Q} = A\varepsilon\sigma T^4 \tag{1}$$

In a system with parallel surfaces, as it represents for instance the double wall without fill material, the heat flux emitted or absorbed from a surface can be estimated by Eq. (2) regarding the individual properties of the surfaces with the indexes 1 and 2 (Christiansen, 1883).

$$\dot{Q_1} = -\dot{Q_2} = \frac{A\sigma(T_1^4 - T_2^4)}{\frac{1}{\varepsilon_1(T_1)} + \frac{1}{\varepsilon_2(T_2)} - 1} \tag{2}$$

The surface-dependent properties can be substituted by the effective

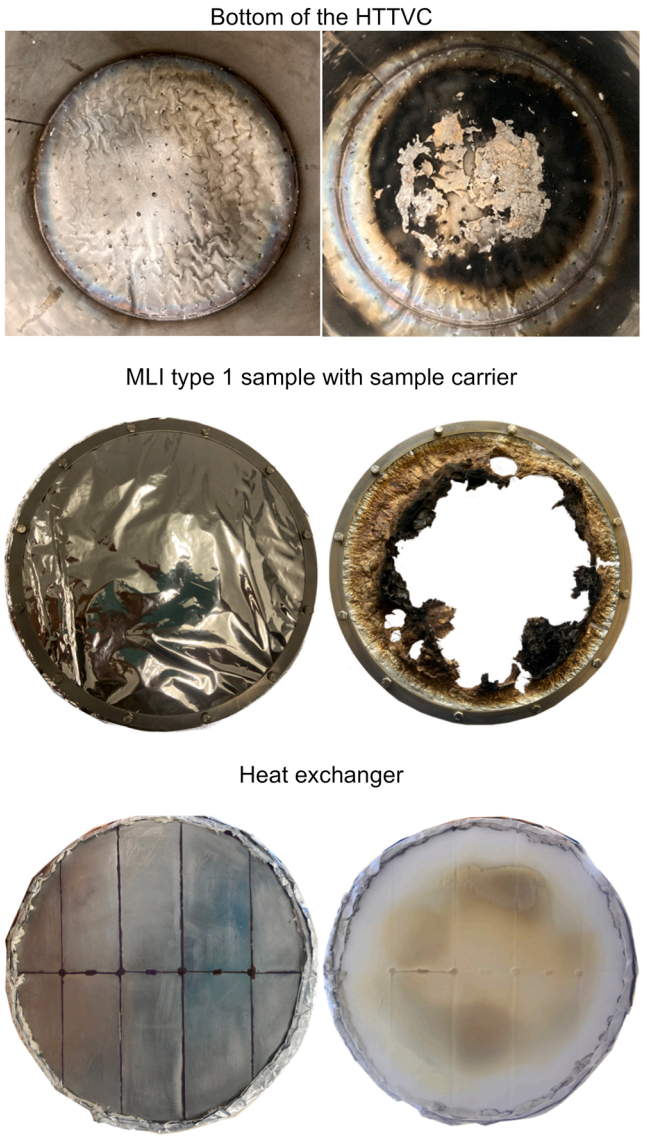

Fig. 4. Tests on MLI type 1: sample and HTTVC components before (left) and after (right) the test.

emissivity ε_{eff} according to Eq. (3) or while regarding an MLI as fill material in between the double wall according to Eq. (4), where 1 and 2 are the indexes of the outer walls, N is the total number of reflecting layers of the MLI, n represents the index of a layer, and ε_{n1} is the emissivity of layer n orientated to surface 1, and ε_{n2} is the emissivity of the layer n orientated to surface 2 (Howell, 2020).

$$\frac{1}{\varepsilon_{eff}} = \frac{1}{\varepsilon_1(T_1)} + \frac{1}{\varepsilon_1(T_1)} - 1 \tag{3}$$

$$\frac{1}{\varepsilon_{eff}} = \frac{1}{\varepsilon_1} + \frac{1}{\varepsilon_2} - 1 + \sum_{n=1}^{N}\left(\frac{1}{\varepsilon_{n1}} + \frac{1}{\varepsilon_{n2}} - 1\right) \tag{4}$$

Regarding the effective emissivity the heat flux $\dot{Q}_1$ can be calculated by Eq. (5).

$$\dot{Q}_1 = -\dot{Q}_2 = A\varepsilon_{eff}\sigma(T_1^4 - T_2^4) \tag{5}$$

Regarding Eq. (5), the effective emissivity ε_{eff} can be also estimated from a known heat flux $\dot{Q}_1$ and the temperatures T_1 and T_2 of the wall surfaces by Eq. (6).

$$\varepsilon_{eff} = \frac{\dot{Q}_1}{A\sigma(T_1^4 - T_2^4)} \tag{6}$$

In this concern the effective emissivity can be applied as a key performance indicator for vacuum-based insulations, which also enables the evaluation of different filling materials.

3. Test equipment

The test equipment consists of the High-Temperature Thermal Vacuum Chamber (HTTVC) where diverse TSI systems can be tested, a heating and cooling system for the HTTVC, a vacuum pump, a water supply system that is used to measure the heat flow through the TSI for instance, and a data acquisition system.

3.1. The HTTVC

The HTTVC shown in Fig. 2 in a sectional view, has a length of 600 mm and an outer diameter of 320 mm. The bottom and the heat exchanger in the HTTVC represent two walls in parallel with a adjustable space of up to 300 mm in between. This concept enables tests with different TSIs at typical installation conditions.

The basis for the thermal loading of TSI samples is the bottom of the HTTVC. This is 12 mm thick and has a radial hole that allows placing a thermocouple near the center of the bottom, which is used to measure the heated wall temperature. The bottom inside of the HTTVC is coated with austenitic steel type 316 L. This represents a material often used in tanks for cryogenic fluids according to ADR, (2023) or UN ECE R-110, 2018 and differs a lot in its radiative properties from other types of steel (Paloposki and Liedquist, 2005).

With the heat exchanger the heat flow through the TSI is measured. This is based on a 1 mm thick copper plate, which is equivalent to the bottom of the HTTVC one side coated with austenitic steel type 316 L. The other side is connected to a copper-spiral tube, which can be supported by a fluid for which the temperature at the inlet and outlet of the spiral can be measured. The heat flow transported by the fluid within the spiral ($\dot{Q}_f$) results from Eq. (7) with the temperature of the fluid at the inlet (T_{fi}), and the outlet (T_{fo}), its specific heat capacity (c_f) which was assumed at 4190 J/kg/k, and its mass flow ($\dot{m}_f$).

$$\dot{Q}_f = \left(T_{fi} - T_{fo}\right)c_f\dot{m}_f \tag{7}$$

The heat exchanger is used to measure heat flows coming from the bottom of the HTTVC. For this reason, all other directions of the heat exchanger are covered with non-combustible and non-heat-sensitive insulation material.

Furthermore, there is a heat shield in the HTTVC, which has the aims:

- to hold and position MLI samples,
- to reduce undefined heat flow from the bottom or the wall of the HTTVC to the heat exchanger,
- to define the geometry and surface where an MLI sample and the heat exchanger do radiative heat exchange with the bottom of the HTTVC.

The heat shield is based on a copper pot which has an outer diameter of 280 mm, and a flat bottom with a circular opening with a diameter of 230 mm. The inner wall of the heat shield is connected to a 6 mm tube from copper, which can be supported by a fluid to control the temperature of the heat shield.

The MLI samples are attached to a sample carrier that fits into the bottom of the heat shield. The sample carrier is based on a ring of stainless steel with an outer diameter of 250 mm, an inner diameter of 230 mm, which has a thickness of 1 mm. To reproduce the mounting condition of a sample under real conditions it is attached to the sample carrier with 12 screws and nuts with a space of some millimeters in

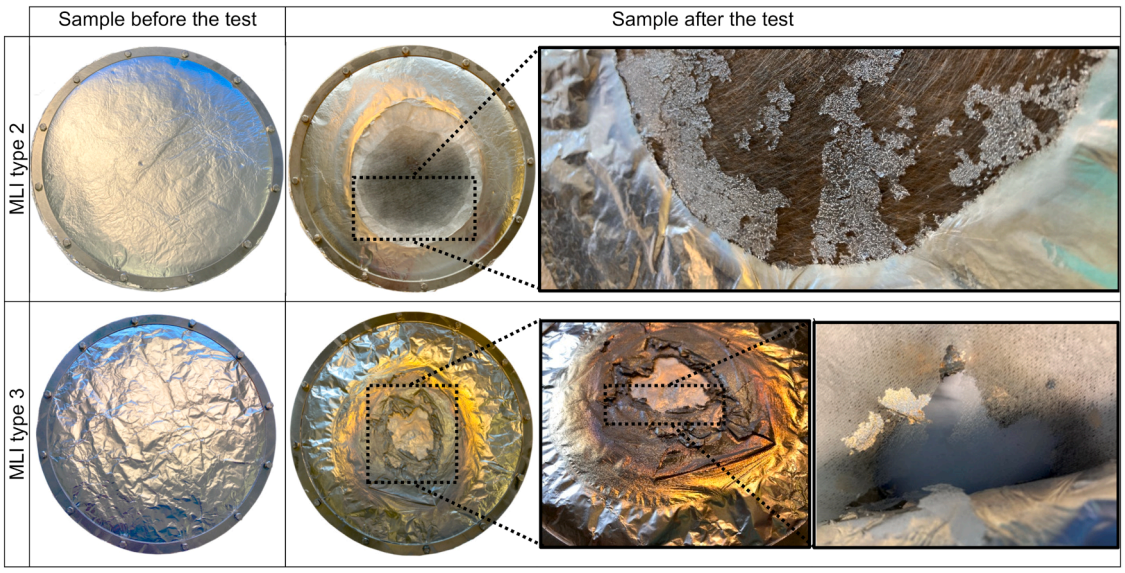

Fig. 5. Samples from the MLI type 2 and MLI type 3 test before (left) and after thermal loading (right).

between. By this construction, a sample is not clamped and the heat flow based on conductivity is low (Gilmore, 2002).

The wall of the HTTVC has a thickness of 8 mm and an outer diameter of 320 mm. To reduce the overall heating of the HTTVC several measures were taken, for instance, to protect gaskets from excessive heating. First, the outer surface of the wall is coated with a high-temperature resistant coating with a high emissivity which increases the amount of energy that is radiated to the environment while testing. Second, the wall-thickness is reduced to 4 mm about the circumstance of the wall about 100 mm in length, at a distance of 100 mm to the bottom of the HTTVC. This measure reduces the heat flow by conduction to the top cover.

From the top cover, the support by fluids is organized (vacuum, heat exchanger, heat shield), the pressure is monitored, samples can be handled, the activities inside the HTTVC can be visually monitored, and it allows cleaning the interior of the HTTVC from residuals of a test sample. To generate a vacuum in the HTTVC a single-level vacuum pump with a minimum absolute pressure of 2 Pa was used.

3.2. The heating system

The heating occurs electrically by an inverter heat treatment unit and two layers of two heating mats. This setup supports the tests with a maximum heating power of 10.5 kW. A maximum specific heat flow of up to 100 kW/m^2 can be achieved, concerning the bottom area of the HTTVC. With this concept the testing can be performed according to different design fires, e.g. ISO 834-1, 1999 (ISO Curve), EN 1991-1-2, 2021 (Hydrocarbon Curve), RABT, 2006 (ZTV Curve), or ISO 21843, 2023. The electrical heating system has the advantage that the test temperature can be better regulated and is much more stable compared to a real fire. The control of the heating power is done by measuring the temperature of the heating wire of a heating mat.

3.3. The cooling system

The HTTVC must be cooled to the initial temperature of the experimental run after the thermal loading of a TSI sample, to evaluate the pressure build-up within the test, e.g. coming from pyrolysis of the test sample, and thermodynamics of gases. For cooling the HTTVC a water-supplied heat exchanger is used.

3.4. The water supply system

The heat shield, heat exchanger in the HTTVC, and also the heat exchanger for cooling the HTTVC are supported with water as fluid. For measuring the heat flow a constant mass flow with constant inlet temperature are important. This is organized firstly by a 1 m^3 storage tank for water and secondly by a balance system, which measures the amount of water flowing through the heat exchanger. Within an experiment, the mass flow will not be changed.

3.5. Data acquisition

For measuring temperatures type K thermocouples were used at the following places:

- at a heating wire of the heating mat,
- between the heating mat layers,
- in the bottom of the HTTVC,
- at the inlet and outlet of the heat exchanger,
- at the outlet temperature of the heat shield,
- and in the environment for measuring the room temperature.

The absolute pressure was measured with a piezo-Pirani sensor type VSR53MV from Thyracont Vacuum Instruments GmbH. For data logging and synchronization of the sensors, an Ahlborn ALMEMO® 2890–9 was applied.

4. Tests

Six tests were carried out with TSI based on vacuum, combined with three different types of MLI, and the three different bulk insulation materials: rock wool, perlite, and microspheres. Within this study, results from a pretest are used, presented with more details in the publication of Eberwein et al. (2023), in which next to vacuum no filling material was applied. Details on the test samples are presented in Table 1.

The heating procedure is divided into three periods. In the first, namely the heating period, the bottom of the HTTVC was heated up with a gradient of approximately 20 K/minute to observe the temperature-dependent behavior of the sample. In the second one, namely the constant bottom-temperature period, a temperature of about 800°C ± 50 K was maintained at the bottom of the HTTVC for 30 minutes, to observe

Fig. 6. Samples from the Rock wool, Perlite and Microspheres test before (left) and after thermal loading (right).

the time-dependent behavior at high temperatures. The magnitude of the temperature was defined based on the outer wall temperature measured on a tank for a cryogenic fluid in a fully engulfing hydrocarbon fire test (Kamperveen et al., 2016). In the third period, namely the cool-down period, the HTTVC was cooled down for about 40 minutes. This was obtained by removing the HTTVC from the heating system and placing it on the cooling system.

5. Results and discussion

The temperatures measured in the bottom of the HTTVC, the calculated heat flow between the bottom and the heat exchanger, and the measured absolute pressure in the HTTVC over time for the six tests with TSI and the Pretest are shown in Fig. 3. The bottom-temperature is the basis for the thermal loading of the TSI samples. The heating mats control system allowed to achieve nearly the same and constant heating rate (20 K/min) in all tests. During the constant bottom-temperature period, in all experiments a constant temperature could be maintained with a tolerance of ± 5 K for 30 min. The differences in the achieved maximum temperature reported in Fig. 3, varying between 770°C to 830°C depend on the insulation performance of each TSI system: the higher the measured heat flow, the lower the bottom temperature.

In the test with MLI type 1 and in the Pretest the lowest maximum temperatures in the constant bottom-temperature period were achieved (approximately 770 °C and 740 °C, respectively). However, the largest heat flows of all tests were observed in these tests. The reason for such

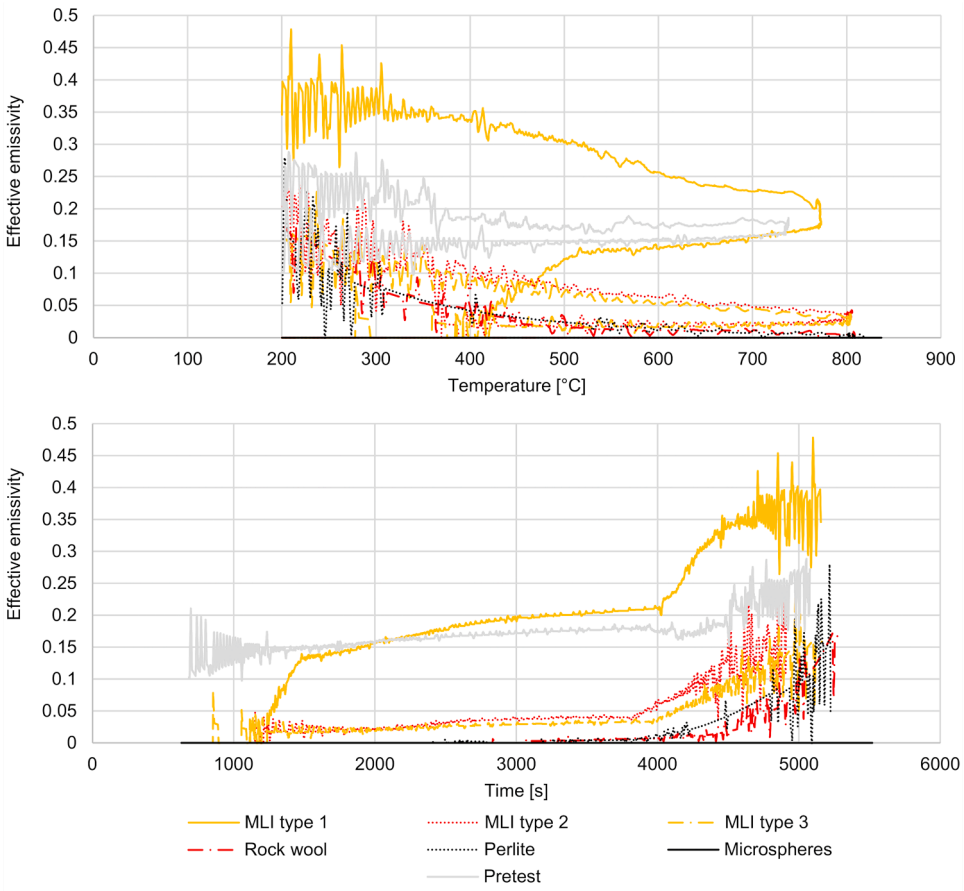

Fig. 7. Effective emissivity in the tests over time and temperature.

behavior can be the not existing fill-mateial in the Pretest and the strongest degradation of all tested samples within the MLI type 1 test represented in Fig. 4, Fig. 5, and Fig. 6, which show the test samples before and after the tests. Of all the test samples, only the sample in the MLI type 1 test has gaps in the thermal insulation after testing. This allows the direct radiant heat transfer between the bottom and the heat exchanger, a condition which is similar to the Pretest, where there was only vacuum in the interspace of the double wall. During the MLI type 1 test, the sample lost 9.8 g in weight (i.e. 65% of its weight before the test). The weight loss is accompanied by the release of pyrolysis products which have a significant influence on the potential achievable heat flow in a fire scenario. These products accumulate on cold surfaces such as the heat exchanger surface and pyrolyze further on warm surfaces such as the bottom surface. The deposition and pyrolysis processes are associated with a change in the surface properties. Here, the emissivity of the inner and outer wall increases which promotes the heat exchange by radiation and thus increases the overall heat flow. A comparison of components before and after the MLI type 1 test is shown in Fig. 4. Further details on the phenomena are presented in Eberwein et al. (2023), where it is also observed that the test scenario does not yet represent the worst case. In consequence, up to 3.5 times higher heat flows could be possible, which could result in a specific peak heat flow of 48 kW/m^2 for the polyester-based MLI, regarding the thermally loaded surface area of the sample of 0.042 m^2.

The results from the MLI type 2 and MLI type 3 tests are significantly different from those of the MLI type 1 test. Fig. 5 shows that the samples only failed locally and not over the entire sample as was observed in the MLI type 1 test. In addition, the degree of damage to a layer decreased with its position on the layer stack, i.e. the degree of damage was higher for the layers closer to the bottom of the HTTVC. Overall, of the 10 aluminum layers, 7 were damaged in the MLI type 2 test, while 4 were damaged in the MLI type 3 test. In comparison, all MLI type 1 layers were damaged due to thermal degradation of the polyester, which occurs starting from approximately 400°C (Bautista et al., 2018). MLI types 2 and 3, on the other hand, are based on layers of pure aluminum and spacers based on glass fibers, which have significantly higher melting points than 400°C. This is also evident from the loss of mass of the samples after the test, which was 0.5 g (2% of weight before the test) for MLI Type 2 and 0.2 g (1% of weight before the test) for MLI type 3. In both tests, no changes were observed on the heat exchanger surface exposed to the samples. At the bottom of the HTTVC residual fragments of the damaged MLI and annealing colors as a result of thermal stress were observed. The latter causes a slight increase in the emissivity coefficient of the inner bottom surface, as shown in Eberwein et al. (2023) for the Pretest. All these effects together result in a significantly lower heat flow in a fire scenario compared to MLI type 1. Within the MLI type 2 test a specific peak heat flow of 3 kW/m^2 and in the MLI type 3 test of 2.4 kW/m^2 respectively were observed.

By far the lowest specific peak heat flow was observed in the Microspheres test with 0.02 kW/m^2, followed by the Rock wool and Perlite test with 0.4 kW/m^2 each. The measurement results and calculations show that these insulation materials significantly reduce the heat flow in a fire scenario compared to the MLI-based TSIs and that the time until a significant heat flow was measured at the inner tank can be significantly increased. This was about halfway of the constant bottom-temperature period and thus about 60 minutes after the start of the test. These results confirm the observations published by van Wingerden et al. (2022) from the Sh2ift project, regarding two tanks with perlite and one with MLI, similar to the aluminium-based MLI with glass-fliess (MLI type 2) regarded in this study. In the three fire tests, the largest heat flow from the fire into the liquid-stored hydrogen was observed in the MLI-insulated tank, where bursting ultimately occurred, which was not

observed in the perlite-insulated tanks.

Within the Perlite test the insulation material, and the heat exchanger do not show structural changes. The perlite next to the heat exchanger was light-yellow discolored. Furthermore, there were the typical annealing colors at the bottom of the HTTVC. After the Rock wool test, the insulation material close to the bottom was discolored, which is shown in Fig. 6, and the stiffness of the discolored rock wool was increased. Within this test accumulates an oily fluid at the heat exchanger and at the sample close to the heat exchanger. This fluid had a light-yellow color. The bottom of the HTTVC shows annealing colors. After the Microspheres test, the initial loose glass spheres were sintered and formed a 10 mm to 15 mm thick plate. This plate and the insulation material close to it were discolored within the test from initial white to light yellow, which is shown in Fig. 6. The bottom of the HTTVC shows annealing colors. The heat exchanger does not show any visual changes.

Within all tests the absolute pressure in the HTTVC was measured, which shows over time Fig. 3. The initial absolute pressure in the HTTVC was in any experiment lower than 0.2 kPa and the leakage was estimated lower than 0.01 Pa/s during a period of 10 minutes before thermal testing. While heating the HTTVC the absolute pressure increases in all tests and also in the Pretest which was done without a test sample. As reasons for the pressure increase are assumed the expansion of residual gases with increasing temperature, and the thermal bakeout, which is for each test similar. Within the Pretest the smallest peak pressure from all tests was observed with 1.4 kPa, which decreases while cooling the HTTVC to initial conditions to 0.8 kPa. The largest peak pressure of 6.6 kPa was observed in the test with MLI type 1, where the release of large amounts of pyrolysis products is also evident from visual analysis. On the other side the MLI type 2 and MLI type 3 test results in peak pressures slightly higher than observed in the Pretest. An argument therefore is the low amount of adhesives, which can pyrolyse, and which are applied in the spacers from glass-fleece or glass-paper. The second-highest peak pressure of 3.3 kPa was observed in the Rock wool test. In this test, the visual comparison of the insulation before and after the thermal load indicates pyrolysis processes in the test. In the third position was the Perlite test which also shows a local light-yellow discoloration and results in a pressure of 2.7 kPa. A similar peak pressure with 2.5 kPa was achieved in the Microspheres test. In this test the strongest pressure change from the tested bulk materials was observed within the cool-down period of the experiment.

Within all tests the pressure increases in the heating and in the constant bottom-temperature period. The pressure is related to the number of gas molecules in the HTTVC and its temperature. An increase in the pressure increases the heat transfer by gas convection and gas conduction (Verschoor et al., 1952). So, the pressure increase can also be a reason for the increasing heat flow in the constant bottom-temperature period of all tests presented in Fig. 3, but especially by the tests regarding different types of MLI, and in the Pretest.

In industrial conditions, the pressure development in the double wall can be different. First, in the HTTVC the volume for the gasses per heated surface area is much bigger and so the increase of pressure is smaller compared to the industrial application. Second, under cryogenic conditions, there is a possibility that residual gases from pyrolysis will condense or freeze at the inner wall, and thus may not be involved in the pressure buildup.

The heat flows calculated for the tests are strongly temperature-dependent. To make the test results more comparable and to transfer the findings to other conditions the effective emissivity can be used. Other conditions may represent a lower temperature of the outer wall, as a result of a different fire impingement and/or lower temperatures at the inner wall e.g. due to the cryogenic transported fluid. The effective emissivity of each tested TSI was calculated by Eq. (6) from the calculated heat flow, the measured temperatures, and the measurement area of 0.042 m^2, and is shown in Fig. 7 over time, and temperature.

The effective emissivity provides quantitative information about the condition of the system. Since the effective emissivity depends on the temperature of the surfaces in the system, measurement data from three representative thermocouples were used to determine it, which are inherently subject to errors. This can be for instance, inhomogeneity in the surface temperature, the uncertainty of measured heat flow through the water system, and simplifications such as ignoring the heat exchangers heat capacity. In conclusion, errors occur especially in transient processes and the method can be used especially to evaluate the state of the system when the temperature is constant, which is given in the constant bottom-temperature period. Also, it has been mentioned that the effective emissivity according to Eq. (6) depends on the size of the measurement area and so also from the residuals as observed within the MLI type 1 test. Due to this aspect, the effective emissivity is also representative for real-life accident scenarios. The data indicates that all MLI-based TSIs change their properties more or less when the bottom-temperature increases above 400°C. This is a typical threshold value for the thermal decomposition of organic materials which are polyester or adhesives. The last ones are applied to carry glass fibers in MLI type 2 and MLI type 3.

6. Conclusion

A high-temperature thermal vacuum chamber (HTTVC) was used to study the behavior of six samples of TSI in a fire scenario. Three different types of MLI were tested, and the bulk insulations were based on rock wool, perlites, and microspheres, each in combination with vacuum. The HTTVC allows testing a TSI at high temperatures and measuring the heat flow through the TSI while thermal loading.

The worst performance of a TSI within a fire scenario was observed from MLI based on polyester (MLI type 1) and vacuum. The insulation degrades when the HTTVC temperature of the bottom increases above 400°C. The pyrolysis products change TSI performance such that the potential heat flow in the fire scenario is higher than in the same system without the MLI. Also, it was observed that, as a consequence of the pyrolysis, the pressure increases and reduces the vacuum. This increases the contribution of gas conduction and convection to the overall heat transfer.

The MLI samples which are based on aluminium layers, and glass-fleece, or glass-paper show much better performance under the thermal loading compared to the polyester-based MLI. These samples were partially damaged in the test and the observed heat flow was much smaller.

From the TSIs based on bulk insulation materials, the microspheres/vacuum insulation has the best performance. This insulation showed a minor degradation within the test, the pressure development was less compared to the other bulk insulations, and the heat flow by the double wall while testing and after testing was nearly unaffected by the fire scenario. Furthermore, the Perlites and Rock wool tests show a good performance in the simulated fire scenario with a similar heat flow, which was 20 times that observed in the Microspheres test. In all tests with bulk insulations, a larger delay between the start of the test and the increase of the heat flow by the double wall was observed compared to the tests with MLI/vacuum insulations.

The results are relevant for the evaluation of accident scenarios involving full-scale cryogenic tanks for LH2 or LNG for instance, and can thus contribute to the improvement of TSI, the development of safer tank designs, as well as the development and definition of emergency measures for the protection of persons and infrastructures.

CRediT authorship contribution statement

Valerio Cozzani: Funding acquisition, Project administration, Supervision, Writing – original draft, Writing – review & editing. **Giordano Emrys Scarponi:** Formal analysis, Investigation, Methodology, Resources, Validation, Writing – original draft, Writing – review & editing. **Davide Camplese:** Data curation, Investigation, Validation, Writing – review & editing. **Aliasghar Hajhariri:** Data curation,

Investigation, Validation, Writing – review & editing. **Robert Eberwein:** Investigation, Methodology, Resources, Validation, Writing – original draft, Writing – review & editing. **Frank Otremba:** Funding acquisition, Project administration, Supervision, Writing – original draft, Writing – review & editing.

Declaration of Competing Interest

The authors declare that they have no known competing financial interests or personal relationships that could have appeared to influence the work reported in this paper.

Acknowledgments

The authors wish to acknowledge the financial support of the research from the German Federal Ministry for Economic Affairs and Climate.

References

Adler, E.J., Martins, J.R.R.A., 2023. Hydrogen-Powered Aircraft: Fundamental Concepts, Key Technologies, and Environmental Impacts. Prog. Aerosp. Sci. 1–59. https://doi.org/10.1016/j.paerosci.2023.100922.

ADR, 2023 - Agreement concerning the International Carriage of Dangerous Goods by Road, United Nations, New York.

Bartlok, G., 2006, Session 3.1: Cryogenic Storage Systems, Lectures, Eurocourse StorHy Train-In 2006, Ingolstadt.

Bautista, Y., Gozalbo, A., Mestre, S., Sanz, V., 2018. Thermal degradation mechanism of a thermostable polyester stabilized with an open-cage oligomeric silsesquioxane. Materials 11 (22), 1–13. https://doi.org/10.3390/ma11010022.

Bradley, I., Scarponi, G.E., Otremba, F., Birk, A.M., 2021. An overview of test standards and regulations relevant to the fire testing of pressure vessels. Process Saf. Environ. Prot. 145, 150–156. https://doi.org/10.1016/j.psep.2020.07.047.

Camplese, D., Chianese, C., Scarponi, G.E., Eberwein, R., Otremba, F., Cozzani, V., 2023. Analysis of high temperature degradation of multi-layer insulation (MLI) systems for liquid hydrogen storage tanks. CEt Vol. 99, 415–420. https://doi.org/10.3303/CET2399070.

Cavallari, et al., 1989, Pressure Protection Against Vacuum Failures on the Cryostats for Lep SC Cavities, Proc. 4th Workshop on RF Superconductivity, pp. 781-803 Tsukuba, Japan.

Christiansen, C., 1883. Absolute Determination of the Heat Emission and Absorption Capacity. Ann. Phys. Wied. Vol.19.

Eberwein, R., 2021, Investigation of the Hazards to People and Structures in Consequence of Failures with LNG Fuel Tanks for Vehicles in Tunnels, PhD-Thesis, TU-Berlin, Berlin.

Eberwein, R., Hajhariri, A., Camplese, D., Scarponi, G.E., Cozzani, V., Otremba, F., 2023. Insulation Materials Used In Tanks For The Storage Of Cryogenic Fluids In Fire Scenarios. Proc. PVP 2023, 1–8. https://doi.org/10.1115/PVP2023-105201.

EN 1991-1-2, 2021, Eurocode 1: Actions on structures - Part 1-2: General actions - Actions on structures exposed to fire.

Gilmore, D.G., 2002, Spacekraft Thermal Control Handbook, Volume I: Fundamental Technologies, 2nd Edition, The Aerospace Press; El Segundo, California.

Horvat, A., 2018. CFD methodology for simulation of LNG spills and rapid phase transition (RPT). Process Saf. Environ. 120, 358–369. https://doi.org/10.1016/j.psep.2018.09.025.

Howell, J.R., 2020. Thermal radiation heat transfer, Vol. 7. CRC Press.

Iannaccone, T., Scarponi, G.E., Landucci, G., Cozzani, V., 2021. Numerical simulation of LNG tanks exposed to fire. Process Saf. Environ. 149, 735–749. https://doi.org/10.1016/j.psep.2021.03.027.

IEA, International Energy Agency, 2022, Global Hydrogen Review, ⟨www.iea.org⟩.

ISO 21843, 2023, Determination of the resistance to hydrocarbon pool fires of fire protection materials and systems for pressure vessels.

ISO 834-1, 1999, Fire-resistance tests - Elements of building construction - Part 1: General requirements.

Jäkel, C., 2018, Development, Validation and Safety-related Application of a Numerical Distribution Model for Liquid Hydrogen, RWTH Aachen, PhD-Thesis.

Kamperveen, J.P., Spruijt, M.P.N., Reinders, J.E.A., 2016, Heat load resistance of cryogenic storage tanks – Results of LNG Safety Program, TNO Report.

Konersmann, R., Reich, F., Balke, C., 2014. Zu den Risiken des Transports von Flüssigerdgas mit Straßentankwagen. Tech. Sicherh., Band. 4, 37–43.

Lehmann, W., Zahn, G., 1978. Safety Aspects for Lhe Cryostats and Lhe Transport Containers, 7. CEC, London.

Lisowski, E., Lisowski, F., 2018. Influence of vacuum level on insulation thermal performance for LNG cryogenic road tankers, ICCHMT 2018. MATEC Web Conf. Volume 240, 1–4. https://doi.org/10.1051/matecconf/201824001019.

Luan, X., Zhang, M., Zhao, S., Zhang, B., 2023. Numerical study on the effects of bund on liquid pool spreading and vapor dispersion after a catastrophic LNG tank failure. Process Saf. Environ. 176, 74–86. https://doi.org/10.1016/j.psep.2023.06.006.

Mital, S.K., Gyekenyesi, J.Z., Arnold, S.M., Sullivan, R.M., Manderscheid, J.M., Murthy, P.L.N., 2006, Review of Current State of the Art and Key Design Issues LH2, NASA/TM—2006-214346.

Paloposki, T., Liedquist, L., 2005, Steel emissivity at high temperatures, Research Notes 2299, VTT Tiedotteita, Otamedia Oy, Espoo.

Pehr, K., 1996a. Aspects Of Safety And Acceptance Of LH2 Tank Systems In Passenger Cars. Ing. J. Hydrog. Energy Vol. 21 (5), 387–395. https://doi.org/10.1016/0360-3199(95)00092-5.

Pehr, K., 1996b, Experimental examinations on the worst-case behaviour of LH2/LNG tanks for passenger cars. Proc. 11th World Hydrogen Energy Conference, pp. Stuttgart.

Peschka, W., 1992. Liquid Hydrogen – Fuel of the Future. Springer-Verlag, Wien New York.

Planas, E., Gasulla, N., Ventosa, A., Casal, J., 2004. Explosion of a road tanker containing liquified natural gas, pp. 315-312 JLP 17. https://doi.org/10.1016/j.jlp.2004.05.005.

Planas, E., Pastor, E., Casal, J., Bonilla, J.M., 2015. Analysis of the boiling liquid expanding vapor explosion (BLEVE) of a liquefied natural gas road tanker: The Zarzalico accident. JLP 34, 127–138. https://doi.org/10.1016/j.jlp.2015.01.026.

RABT, 2006, Richtlinien für die Ausstattung und den Betrieb von Straßentunneln. Forschungsgesellschaft für Straßen- und Verkehrswesen.

Salzano, E., Carboni, M., Pio, G., 2020. The effects of low-temperature phenomena on rapid phase transition of liquid hydrogen. Int. J. Hydrog. Energy 45, 32676–32685. https://doi.org/10.1016/j.ijhydene.2020.08.140.

Scarponi, G.E., Landucci, G., Tugnoli, A., Cozzani, V., Birk, A.M., 2017. Performance assessment of thermal protection coatings of hazardous material tankers in the presence of defects. Process Saf. Environ. Prot. 105, 393–409. https://doi.org/10.1016/j.psep.2016.10.009.

Tugnoli, A., Cozzani, V., Di Padova, A., Barbaresi, T., Tallone, F., 2012. Mitigation of fire damage and escalation by fireproofing: A risk-based strategy. Reliab. Eng. Syst. Saf. 105, 25–35. https://doi.org/10.1016/j.ress.2011.11.002.

UN ECE R-110, 2018, Rev. 4.

Ustolin, F., Giannini, L., Collina, G., Tincani, G., Salzano, E., Cozzani, V., 2023, Consequences Of Liquid Hydrogen Tank Explosions, Proc. 10. ICHS, pp. 411-422 Québec City.

Ustolin, F., Iannaccone, T., Cozzani, V., Jafarzadeh, S., Paltrinieri, N., 2021, Time to Failure Estimation of Cryogenic Liquefied Tanks Exposed to a Fire, ESREL 2021, pp. 935-942, Singapore, DOI:10.3850/978-981-18-2016-8_182-cd.

Ustolin, F., Scarponi, G.E., Iannaccone, T., Cozzani, V., Paltrinieria, N., 2022b. Cryogenic Hydrogen Storage Tanks Exposed to Fires: a CFD Study. CEt Vol. 90, 535–540. https://doi.org/10.3303/CET2290090.

Ustolin, F., Tolias, I.C., Giannissi, S.G., Venetsanos, A.G., Paltrinieri, N., 2022a. A CFD analysis of liquefied gas vessel explosions. Process Saf. Environ. 159, 61–75. https://doi.org/10.1016/j.psep.2021.12.048.

van Wingerden, K., Kluge, M., Habib, A.K., Ustolin, F., Paltrinieri, N., 2022, Medium-scale tests to investigate the possibility and effects of BLEVEs of storage vessels containing liquified hydrogen, 17th EFCE, Prague, pp.1-6, https://doi.org/10.3303/CET2290092.

Verschoor, J.D., Greebler, P., Manville, N.J., 1952. Heat Transfer by Gas Conduction and Radiation in Fibrous Insulations. Trans. Am. Soc. Mech. Eng. 74 (6), 961–967.

Vollmacher, K., 2018. Accid. Involv. LNG Truck, CTIF Comm. Extrication N. Technol. 2018.

Wiseman, M., Crawford, K., Drury, M., Jordan, K., Preble, J., Saulter, Q. Schneider, W., 1994, Loss of Cavity Vacuum Experiment at CEBAF, ICMC 1993, pp. 997-1003 Albuquerque, New Mexico.

Xu, Z., Jordan, T., Friedrich, A., Vagts, S., Friese, P., Adamczyk, A., 2023, Heat And Mass Transfer Modeling Of Vacuum Insulated Vessel Storing Cryogenic Liquid In Loss Of Vacuum Accident, Proc. 10. ICHS, pp. 461-472, Québec City.